Correlation between rare-earth oscillator strengths and rare-earth–valence-band interactions in neodymium-doped YMO_4 (M=V, P, As), $Y_3Al_5O_{12}$, and $LiYF_4$ matrices

O. Guillot-Noel
Ecole Nationale Supérieure de Chimie de Paris (ENSCP), Laboratoire de Chimie Appliquée de L'Etat Solide, UMR-CNRS 7574, 11 rue Pierre et Marie Curie, 75231 Paris Cedex 05, France

B. Bellamy
Ecole Nationale Supérieure de Chimie de Paris (ENSCP), Laboratoire de Physico-Chimie des Surfaces, ESA-CNRS 7045, 11 rue Pierre et Marie Curie, 75231 Paris Cedex 05, France

B. Viana and D. Gourier
Ecole Nationale Supérieure de Chimie de Paris (ENSCP), Laboratoire de Chimie Appliquée de L'Etat Solide, UMR-CNRS 7574, 11 rue Pierre et Marie Curie, 75231 Paris Cedex 05, France

(Received 8 September 1998; revised manuscript received 16 February 1999)

Nd^{3+}:YVO_4 is one of the more promising laser hosts for micro and diode-pumped solid-state lasers. At room temperature, Nd^{3+} ions in this matrix exhibit strong absorption cross sections sixfold higher than in $Y_3Al_5O_{12}$. The neodymium oscillator strengths are measured in YMO_4 (M=V, P, As), $Y_3Al_5O_{12}$, and $LiYF_4$ hosts, and they increase in the sequence $Y_3Al_5O_{12}<LiYF_4<YAsO_4<YPO_4<YVO_4$. This paper is an attempt to correlate these variations with covalent interactions between neodymium $4f$,$5d$ levels and valence-band levels. The strength of orbital interactions between $4f$ levels and valence-band states is estimated from the analysis of $3d$ x-ray photoemission spectra of Nd^{3+} ions. A two-step model is derived, in which $5d$ admixture into the $4f$ levels of the rare earth occurs via the valence-band levels. This model shows that the oscillator strengths increase with the Nd $4f$-valence-band interactions. [S0163-1829(99)00427-0]

I. INTRODUCTION

Neodymium-doped yttrium orthovanadate Nd^{3+}:YVO_4 is an efficient solid-state laser material, where Nd^{3+} ions exhibit a broad and strong absorption band around 808 nm and a very intense emission around 1 μm. These features allow one to miniaturize this material in diode-pumped microchip lasers.[1–3] Optical properties of Nd^{3+} ions are almost identical in the three zircon-type matrices YVO_4, YPO_4, and $YAsO_4$.[4] At room temperature, the broadening of the Nd^{3+} ions absorption band around 808 nm is homogeneous and can be explained by the specific crystal-field strength in these matrices.[5] In the three zircon-type matrices, neodymium presents a very strong absorption cross section near 808 nm (see Table I), which is five to six times larger in YVO_4 than in $Y_3Al_5O_{12}$. To our knowledge, the origin of this strong absorption is not yet explained. In the case of homogeneously broadened transitions, high transition probabilities could lead to high-absorption cross sections. The aim of this paper is to propose an explanation for the variation of the neodymium oscillator strengths observed in the three YMO_4 (M=V, P, As) matrices and in $Y_3Al_5O_{12}$ and $LiYF_4$ matrices for comparison. An attempt is made to correlate these variations to orbital interactions between the rare-earth levels (i.e., $4f$ and $5d$ levels) and the matrix levels and in particular the valence-band levels (VB levels) which are mainly composed of oxygen and fluorine $2p$ states for oxide and fluoride hosts respectively.

In previous works dealing with crystal-field parameter calculations in oxide hosts, some authors took into consideration the interaction between the lanthanide $4f$ orbitals and the s and p orbitals of the ligands.[6,7] Since the $4f$ levels can always be considered as localized, even in solids presenting very narrow energy gap,[8] covalency is generally introduced as a phenomenological parameter in crystal-field calculations. Optical transitions of a rare-earth ion in a solid matrix occur between states belonging to the same configuration $4f^n$ ($4f^3$ for Nd^{3+}), which are forbidden by the Laporte rule because they involve states with the same parity. In the Judd-Ofelt approach,[9,10] transitions between $4f$ orbitals are slightly allowed by admixture of $5d$ states into $4f$ states induced by odd terms of the crystal-field Hamiltonian. This purely electrostatic approach is justified by the fact that the $4f$-ligand covalency is usually considered as negligible compared to crystal-field effects. In this paper, we propose an-

TABLE I. Absorption cross sections of Nd^{3+} ions around an 800-nm wavelength in YMO_4 (M=V, P, As), $Y_3Al_5O_{12}$, and $LiYF_4$.

	Absorption cross sections (10^{-19} cm^2)		
Host	π polarization	σ polarization	Average polarization
YVO_4	3.8 (808.7 nm)	1.5 (808.7 nm)	2.3
YPO_4	3.5 (803.2 nm)	1.1 (804 nm)	1.9
$YAsO_4$	2.8 (804.8 nm)	0.8 (804.7 nm)	1.5
$LiYF_4$	0.8 (792 nm)	0.3 (797 nm)	0.5
$Y_3Al_5O_{12}$	no polarization		0.6 (795.4 nm)

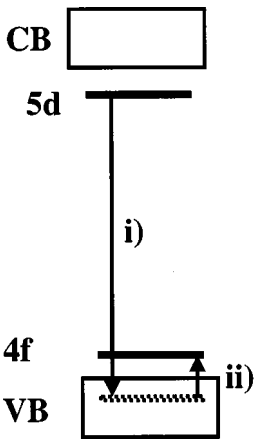

FIG. 1. Schematic representation of the two-step mechanism for the mixing of the Nd $5d$ levels with Nd $4f$ levels via the VB states (i) $5d$-VB interaction, (ii) the $4f$-VB interaction.

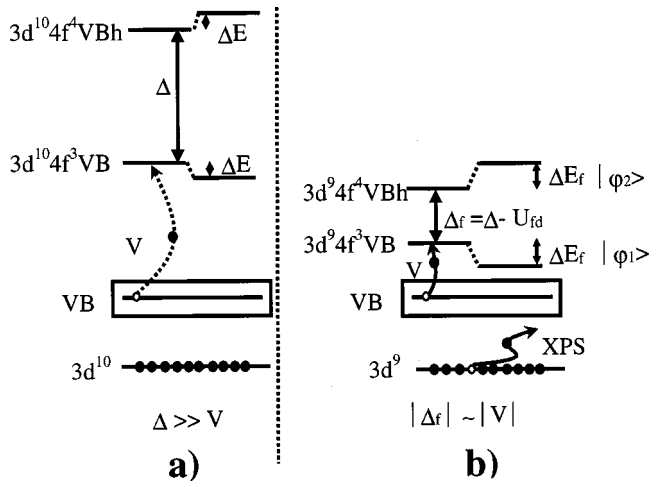

FIG. 2. Initial (a) and final (b) states in a $3d$ XPS transition. In the initial state (a), the covalent interaction between $4f$ and valence-band levels is very small (weak ΔE shift). In the final state (b), the virtual electron transfer between these two levels leads to an interaction between the $3d^9 4f^3$VB and $3d^9 4f^4$VBh configurations (strong ΔE_f shift).

other mechanism of even parity admixture into $4f$ levels that takes into account the electronic structure of the host, and not only the symmetry of the site occupied by the rare-earth ion. The basic idea of this model can be understood by considering the simple energy level diagram shown in Fig. 1, representing schematically the rare-earth energy levels compared to the host energy levels. The essential feature is that the valence-band (VB) levels, composed of oxygen or fluorine $2p$ orbitals, transfer the even parity from the $5d$ to the $4f$ levels via metal-anion covalency. The important radial extension of the rare-earth $5d$ orbitals should be responsible for a significant $5d$-$2p$ covalency, which should produce a $5d$ admixture into VB levels (arrow *i* in Fig. 1). Because the $4f$ levels are energetically close to the VB edge, even a very small $4f$-VB covalency can produce a $2p$ admixture into $4f$ levels (arrow *ii*). A small $5d$ contribution to the VB levels provides a channel through the weak $4f$-VB($2p$,$5d$) covalency to give a small $5d$ admixture into $4f$ levels. The VB levels thus act as a relay in the $5d$-$4f$ mixing via the two-step mechanism $5d \rightarrow \mathrm{VB} \rightarrow 4f$.

To test this hypothesis, it is necessary to measure the variation of the $4f$-$2p$ covalency across a series of compounds. We used photoelectron spectroscopy, and in particular the structure of the $3d$ photoemission spectrum, to estimate these weak interactions.[11–15] The principle of the method is described in Sec. II. After briefly describing the experimental details in Sec. III, the results of photoelectron and optical spectroscopic measurements are discussed in Sec. IV. Finally, Sec. V considers in more detail the correlation between the oscillator strengths of Nd^{3+} optical transitions and the $4f$-VB covalency effects measured by photoelectron spectroscopy, by using a simple perturbative approach.

II. DETERMINATION OF $4f$-LIGAND INTERACTIONS BY PHOTOELECTRON SPECTROSCOPY

X-ray photoemission spectroscopy has become a widely used technique for studying filled electronic energy levels in solids. From the analysis of $3d$ photoelectron signals of rare earth ions, others have shown that it is possible to estimate the strength of the covalent interactions between the rare earth $4f$ levels and the VB levels mainly composed of oxygen or fluorine $2p$ levels by using the impurity Anderson model.[11–15]

The appearance of satellites (secondary signals) in the $3d$ XPS spectrum is due to an electron transfer from the VB levels to the $4f$ shell. To explain the relationship between $3d$ photoemission and Nd $4f$-VB interactions, let us consider the electronic structure of a filled VB and neodymium impurity with $3d^{10}4f^3$ configuration (Fig. 2). We neglect the multiplet coupling effects due for Coulomb and spin-orbit interactions of the $3d$ and $4f$ levels. In the case of neodymium, these multiplet coupling effects are weak in $3d$ XPS, and they lead only to a broadening of the transition and in some cases to minor spectral structures.[11]

Let us first consider the $4f$-VB interactions in the initial state of photoemission before photoionisation of the $3d$ electron [Fig. 2(a)]. An electron can be virtually transferred from the VB-$2p$ states to the $4f$ shell as a result of the weak covalent interaction between these two types of orbitals; this interaction gives rise to the excited $3d^{10}4f^4$VBh configuration, where h refers to a hole in the valence band. The physical signature of this virtual transfer between the fundamental $3d^{10}4f^3$VB and the excited $3d^{10}4f^4$VBh configurations is a shifting (by a value ΔE) of the excited and ground state configurations towards higher and lower energies, respectively [Fig. 2(a)]. The energy difference Δ between these two configurations, the charge transfer V between the VB levels and the $4f$ shell, and the energy shift ΔE arising from the configuration interaction are linked by a second-order perturbation expression

$$\Delta E \propto \frac{V^2}{\Delta}. \tag{1}$$

In the case of Nd_2O_3, characterized by $\Delta = 9.5\,\mathrm{eV}$ and $V = 0.5\,\mathrm{eV}$,[11] the interaction ($\Delta E \approx 0.03\,\mathrm{eV}$) between the $3d^{10}4f^3$VB and $3d^{10}4f^4$VBh configurations is weak; hence, the $4f$-VB covalency is very limited. Therefore, in the ground state of the matrix-Nd^{3+} system [Fig. 2(a)], the

charge transfer between the VB states and the $4f$ shell can be neglected, since ΔE is much smaller than the photoemission linewidth. This initial state can be considered as only composed of the fundamental $3d^{10}4f^3$VB configuration. The very weak covalency is negligible to a first approximation, so it cannot be measured.

In the final state of photoemission, after photoionization of a $3d$ electron [Fig. 2(b)], the $4f$ states are shifted to lower energy by a value $-U_{fd}$, as a hole is created in the $3d$ core levels inducing an attractive potential between the $3d$ core hole and the $4f$ states. In the final state, Δ_f and ΔE_f are the energy differences between the $3d^94f^3$VB and $3d^94f^4$VBh configurations and the energy shift arising from the interaction between these two configurations, respectively [see Fig. 2(b)].

A simple expression of Δ_f is obtained from the impurity Anderson model[11–16]

$$\Delta_f=\Delta-U_{fd} \tag{2}$$

with U_{fd} and Δ being of the same order of magnitude [for Nd_2O_3, $\Delta=9.5$ eV, $U_{fd}=12$ eV (Ref. 11)]. As for the initial state [Eq. (1)], the parameters V, Δ_f, and ΔE_f are related by

$$\Delta E_f \propto \frac{V^2}{\Delta_f}, \tag{3}$$

where a larger value of the ΔE_f relative to its equivalent ΔE in the initial state indicates a stronger $4f$-VB covalency. Therefore, a strong interaction occurs between the $3d^94f^3$VB and $3d^94f^4$VBh configurations, leading to states $|\varphi_1\rangle$ and $|\varphi_2\rangle$ described by the following linear combinations:

$$|\varphi_1\rangle=a|3d^94f^3\mathrm{VB}\rangle+b|3d^94f^4\mathrm{VB}h\rangle,$$
$$|\varphi_2\rangle=b|3d^94f^3\mathrm{VB}\rangle-a|3d^94f^4\mathrm{VB}h\rangle. \tag{4}$$

The interaction between the fundamental and the excited configurations, negligible in the initial state of photoemission (ΔE), is strongly increased in the final state (ΔE_f) by photoionisation of a $3d$ electron. Thus the effect of the covalent interaction (measured by V) is amplified after photoemission of a $3d$ electron.

The $3d$ x-ray photoemission spectroscopy (XPS) is composed of two lines (Fig. 3) corresponding to the two transitions from the initial state $|\varphi_0\rangle=|3d^{10}4f^3\mathrm{VB}\rangle$ to the final states $|\varphi_1\rangle$ and $|\varphi_2\rangle$ given by Eq. (4). From this two-line spectrum, the charge transfer V between the VB$2p$ levels and the Nd$4f$ levels as well as the energy difference between these two levels can be calculated. Two situations are shown in Fig. 3. In the first, the $3d^94f^4$VBh configuration is at a lower energy than the $3d^94f^3$VB configuration without configuration interaction, which corresponds to $|U_{fd}|>\Delta$ and $\Delta_f<0$ in Eq. (3) [see Fig. 3(a)]. In the second, the $3d^94f^3$VB configuration is at lower energy than the $3d^94f^3$VBh configuration, which corresponds to $|U_{fd}|<\Delta$ and $\Delta_f>0$ in Eq. (2) [see Fig. 3(b)]. In the following, ε_1 and ε_2 are, respectively, the energy of the lowest and the highest configurations, Δ_{exp} is the experimental energy difference between the two XPS transitions and $E_{4f}-E_{\mathrm{VB}}$ is the energy difference between the Nd $4f$ fundamental level and the VB

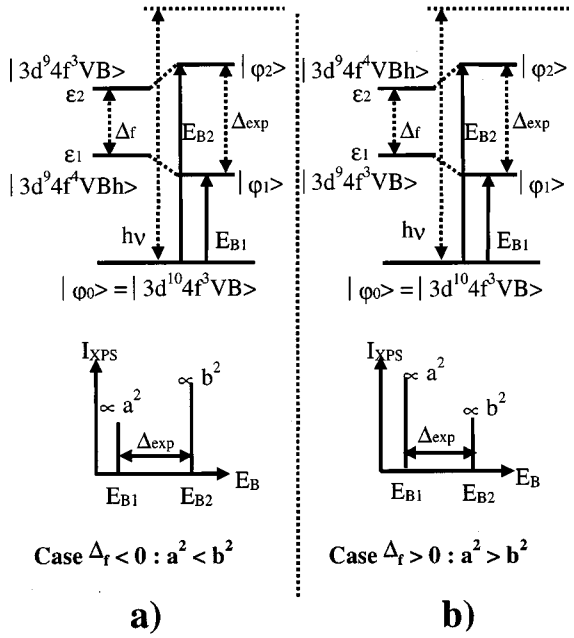

FIG. 3. Energy level diagram for the two-peak structure of a $3d_j$ XPS transition ($j=\frac{5}{2}$ or $\frac{3}{2}$). A schematic x-ray photoemission spectrum is drawn for the two cases: (a) $\Delta_f<0$ and (b) $\Delta_f>0$. $h\nu$ is the energy of the incident x-ray.

states that transfer their electrons to the $4f$ shell (see Fig. 3). The Hamiltonian H_{hyb} describes the interaction between the $3d^94f^3$VB and $3d^94f^4$VBh configurations in the final state of photoemission, and it is represented by the following matrix in the $\{|3d^94f^4\mathrm{VB}h\rangle,|3d^94f^3\mathrm{VB}\rangle\}$ basis set

$$\tilde{H}_{\mathrm{hyb}}=\begin{pmatrix}\varepsilon_1 & V\\ V & \varepsilon_2\end{pmatrix}. \tag{5}$$

From the eigenvalues and the associated eigenvectors $|\varphi_1\rangle$ and $|\varphi_2\rangle$ of this matrix, one obtains the following expressions for Δ_f and V:

$$\Delta_f=\frac{a^2-b^2}{a^2+b^2}\Delta_{\mathrm{exp}}, \tag{6}$$

$$V=\left|\frac{a}{b}\right|\frac{b^2}{a^2+b^2}\Delta_{\mathrm{exp}}, \tag{7}$$

where the coefficients a and b of the states $|\varphi_1\rangle$ and $|\varphi_2\rangle$ are given in expression (4). The transition probabilities for photoemission as a function of the $3d$ binding energy are given by the Fermi golden rule[12]

$$I(E_L)=\sum_{i=1}^{2}|\langle\varphi_i|a_d|3d^{10}4f^n\mathrm{VB}\rangle|^2 \times\frac{w/\pi}{(E_L-E_{Li}+E_{3d^{10}4f^n\mathrm{VB}})^2+w^2}, \tag{8}$$

where w is the linewidth of the Lorentzian photoemission line related to the lifetime of the $3d$ hole. E_{Li} is the binding energy of the $|\varphi_i\rangle$ level and a_d is the annihilation operator

for a $3d$ electron. By using expression (4) for the $|\varphi_i\rangle$ levels, expression (8) for $I(E_L)$ becomes the following:

$$I(E_L)\propto|a|^2\frac{w/\pi}{(E_L-E_{L1}+E_{3d^{10}4f^n\mathrm{VB}})^2+w^2}$$
$$+|b|^2\frac{w/\pi}{(E_L-E_{L2}+E_{3d^{10}4f^n\mathrm{VB}})^2+w^2}. \quad (9)$$

The intensity of the lower binding energy XPS lines, due to $|\varphi_0\rangle\rightarrow|\varphi_1\rangle$ transition, is proportional to a^2 and the intensity of the higher binding energy line, due to the $|\varphi_0\rangle\rightarrow|\varphi_2\rangle$ transition, is proportional to b^2 (see Fig. 3). Therefore, from the energy splitting Δ_{exp} between the two XPS lines and their relative intensities a^2/b^2, parameters Δ_f and V can be calculated by using Eqs. (6) and (7).

It is also possible to estimate the energy of the $4f$ levels with respect to the valence-band level, $E_{4f}-E_{\mathrm{VB}}$, from the $3d$ XPS lines. By using the impurity Anderson model, one obtains the following expression for Δ:[11–16]

$$\Delta=E_{4f}-E_{\mathrm{VB}}+3U_{ff}, \quad (10)$$

where U_{ff} is the Coulomb interaction between $4f$ electrons. The quantity $3U_{ff}$ is the energy of the $4f^3+e^-\rightarrow4f^4$ transition. $E_{4f}-E_{\mathrm{VB}}$ is obtained by substituting Eq. (10) in Eq. (2)

$$E_{4f}-E_{\mathrm{VB}}=\Delta_f+(U_{fd}-3U_{ff}). \quad (11)$$

As a conclusion, the appearance of a two-line structure in the $3d$ XPS of Nd^{3+} ions arises from a weak covalent interaction between the VB-$2p$ levels and the Nd-$4f$ levels. By measuring the relative intensity and the energy difference between these two lines, the VB-$4f$ interaction and the energy splitting $E_{4f}-E_{\mathrm{VB}}$ between the Nd $4f$ levels and the VB levels involved in the interaction can be estimated. Therefore, XPS measurements give an indirect estimate of the interaction between the rare earth ion and its ligands.

III. EXPERIMENTAL DETAILS

XPS measurements were performed in a UHV apparatus consisting of a transfer chamber, a preparation chamber and an analysis chamber, maintained at a pressure smaller than 10^{-8} Pa. A magnetic transfer connects the three chambers. XPS spectra were obtained with a (LEYBOLD LHS10) spectrometer by using Mg Kα or Al Kα radiation ($h\upsilon=1253.6$ eV and $h\upsilon=1486.6$ eV, respectively). In-house software was used for data acquisition and analysis. The C $1s$ peak position at 284.7 eV was used to calibrate the electron-binding energy scale. The spectra were obtained from polycrystalline samples (powders) that were prepared by classical solid-state reactions. The samples were Nd:YMO_4 (M=V, P, As) and Nd:$Y_3Al_5O_{12}$ doped with 5% neodymium and Nd:$LiYF_4$ doped with 10% neodymium.

The neodymium oscillator strengths were calculated from absorption spectra recorded at room temperature in the 430–880-nm range on a Cary 5-Varian spectrometer. The measurements were performed on single crystals grown by the Czochralski method for Nd:$LiYF_4$, Nd:$Y_3Al_5O_{12}$, and Nd:YVO_4 and by the flux method for Nd:YPO_4 and Nd:$YAsO_4$.

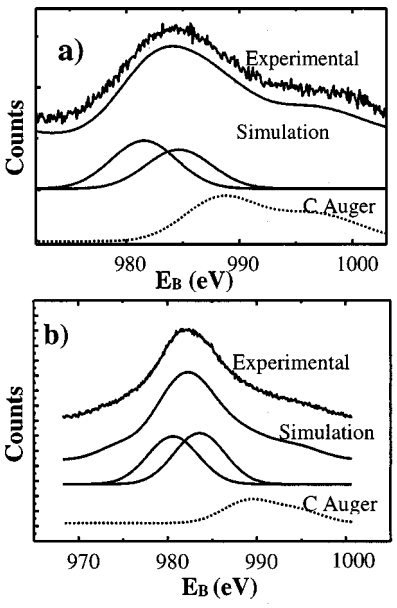

FIG. 4. Experimental and simulated $3d_{5/2}$ XPS transition for Nd^{3+} ions (a) in $Y_3Al_5O_{12}$ with $\Delta_f>0$ and (b) in $LiYF_4$ with $\Delta_f<0$.

IV. RESULTS

A. Photoelectron spectroscopy

The $3d_{5/2}$ XPS lines of the Nd^{3+} ion are shown in Figs. 4(a) and 4(b) for $Y_3Al_5O_{12}$ and $LiYF_4$ matrices, respectively, and in Fig. 5 for the zircon-type matrices. Each spectrum exhibits the expected two-line structure of the Nd sample and a carbon Auger transition from carbon impurities at the sample surface. These impurities constitute an internal reference via the carbon $1s$ signal.

For each simulated spectrum, the two components of the $3d_{5/2}$ signal exhibit a Gaussian shape and an identical width. The width of $3d$ photoemission lines results from a convolution of the natural line shape due to the lifetime of the core-hole in the $3d$ levels and the instrumental line shape. Except for the $Y_3Al_5O_{12}$ host, all of the spectra in Figs. 4 and 5 can be analyzed by a negative Δ_f value [Fig. 3(a)], implying that the $3d^94f^4\mathrm{VB}h$ configuration is at a lower energy than the $3d^94f^3\mathrm{VB}$ configuration.

To obtain the energy splitting $E_{4f}-E_{\mathrm{VB}}$ from Eq. (11), the Δ_f value is corrected by (U_{fd}-$3U_{ff}$) which takes into account the Coulomb interaction $3U_{ff}$ between $4f$ electrons and the core-hole potential U_{fd} acting on the $4f$ electrons. In this paper, we assume that (U_{fd}-$3U_{ff}$) does not vary significantly from Nd metal to Nd oxide and from one host to another. The values measured for neodymium metal are $U_{ff}=0.56$ eV (Ref. 17) and $U_{fd}=6$ eV,[18] which give (U_{fd}-$3U_{ff}$)$=+4.3$ eV. The value of U_{ff} in Nd metal was measured from bremsstrahlung isochromat spectroscopy which gives the energy of the $4f^3+e^-\rightarrow4f^4$ process.

To check the hypothesis of a constant (U_{fd}-$3U_{ff}$) term from Nd metal to Nd in oxide hosts, the $3U_{ff}$ value was estimated from the $3d_{5/2}$ XPS of Nd^{3+} ions in Nd_2O_3 shown in Fig. 6 and from the x-ray absorption spectra (XAS) of Nd_2O_3 given in Ref. 19. A value of 982.5 eV is obtained for the $3d^{10}4f^3\mathrm{VB}\rightarrow3d^94f^3\mathrm{VB}+e^-$ transition from the XPS spectrum and a value of 980.8 eV was found for the

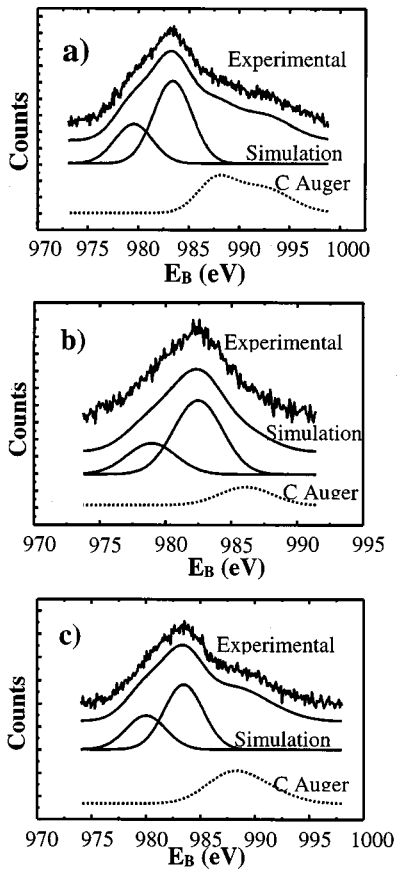

FIG. 5. Experimental and simulated $3d_{5/2}$ XPS transition for Nd^{3+} ions (a) in YVO_4, (b) in YPO_4, and (c) in $YAsO_4$. All the spectra are simulated with a negative Δ_f value.

$3d^{10}4f^3\text{VB}\rightarrow 3d^9 4f^4\text{VB}$ transition from the XAS spectrum. The energy difference 1.7 eV between these two transitions, which is the energy of the $4f^3+e^-\rightarrow 4f^4$ transition (neglecting coupling effects), is close to the value of $3U_{ff}$ measured in Nd metal. All of the experimental parameters Δ_{exp}, a^2/b^2, w, V, Δ_f, and $E_{4f}-E_{\text{VB}}$ deduced from the $3d$ XPS spectra are reported for the five matrices in Table II. For the three zircon-type matrices, the values of Δ_{exp} and a^2/b^2 obtained in this work are in very good agreement with those reported for $NdMO_4$ (M=V, P, As).[15] The high value obtained for the a^2/b^2 ratio in $LiYF_4$ is also in good agreement with the values obtained in several fluoride hosts.[15] From Table II, the charge transfer V between the VB and $4f$ states shows a weak variation through the series. It slightly increases from the more ionic compound $LiYF_4$ to the more covalent compound YVO_4. The energy splitting $E_{4f}-E_{\text{VB}}$ between the $4f$ levels and the VB-$2p$ levels, which interact with the $4f$ states, decreases from $Y_3Al_5O_{12}$ (4.6 eV) to YVO_4 (2.9 eV).

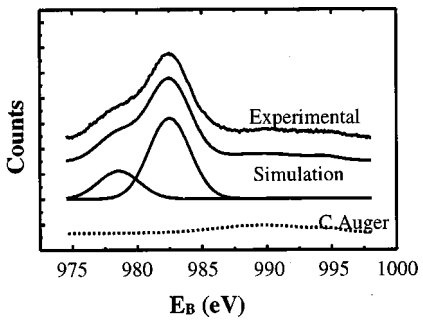

FIG. 6. Experimental and simulated $3d_{5/2}$ XPS transition for Nd^{3+} ions in Nd_2O_3 with $\Delta_f<0$.

B. Oscillator strengths for optical absorption of Nd^{3+}

The oscillator strength $f_{JJ'}^{\text{exp}}$ of a transition between two multiplets $^{2S+1}L_J\rightarrow{}^{2S'+1}L'_{J'}$ is obtained experimentally by the usual formula

$$f_{JJ'}^{\text{exp}}=\frac{2.3mc^2}{\pi e^2}\frac{1}{NL\lambda^2}\int \text{OD}(\lambda)d\lambda, \tag{12}$$

where m and e are the electron mass and charge respectively, $\text{OD}(\lambda)$ is the optical density obtained from absorption measurements, L is the sample thickness, and N the number of absorbing ions per unit volume. In the case of Nd^{3+} ions in the 430–880 nm range, the magnetic dipolar oscillator strength contribution is negligible compared to the electric dipolar contribution. For all the transitions considered in this work, the oscillator strengths have a purely electric dipole character.

The zircon-type and fluoride matrices are anisotropic and measurements were thus performed along the σ and π polarization axes, and we calculated an average oscillator strength according to

TABLE II. Values of the parameters associated to Nd^{3+} ions in YMO_4 (M=V, P, As), $Y_3Al_5O_{12}$ and $LiYF_4$ from the analysis of $3d$ XPS.

Host	Δ_{exp} (eV)	a^2/b^2	w (eV)	Δ_f (eV)	V (eV)	$E_{4f}-E_{\text{VB}}$ (eV)	Ref.
YVO_4	3.9±0.1	0.46±0.03	3.8±0.1	−1.4±0.1	1.81±0.05	2.9±0.1	This work
YPO_4	3.6±0.1	0.42±0.03	3.7±0.1	−1.5±0.1	1.64±0.05	2.9±0.1	This work
$YAsO_4$	3.4±0.1	0.52±0.05	3.5±0.1	−1.1±0.1	1.61±0.05	3.2±0.1	This work
$LiYF_4$	3.0±0.1	0.93±0.03	5.7±0.1	−0.11±0.05	1.50±0.05	4.19±0.05	This work
$Y_3Al_5O_{12}$	3.0±0.1	1.25±0.03	5.8±0.1	+0.33±0.04	1.49±0.05	4.63±0.04	This work
$NdVO_4$	3.7	0.445					15
$NdPO_4$	3.2	0.38					15
$NdAsO_4$	3.35	0.61					15

TABLE III. Values of the oscillator strengths $\overline{f}^{\mathrm{exp}}_{JJ'}$ experimental and $\overline{f}^{\mathrm{calc}}_{JJ'}$ calculated (from the Judd-Ofelt approach) and of Judd-Ofelt parameters for Nd^{3+} ions in YMO_4 (M = V, P, As), $Y_3Al_5O_{12}$, and $LiYF_4$. The experimental values were measured from absorption spectra except for $LiYF_4$ obtained from Ref. 21.

	YVO_4			YPO_4			$YAsO_4$			$LiYF_4$			$Y_3Al_5O_{12}$		
Level	$\overline{f}^{\mathrm{exp}}_{JJ'}$ (in 10^{-6})	$\overline{f}^{\mathrm{calx}}_{JJ'}$ (in 10^{-6})	Err. %	$\overline{f}^{\mathrm{exp}}_{JJ'}$ (in 10^{-6})	$\overline{f}^{\mathrm{calx}}_{JJ'}$ (in 10^{-6})	Err. %	$\overline{f}^{\mathrm{exp}}_{JJ'}$ (in 10^{-6})	$\overline{f}^{\mathrm{calx}}_{JJ'}$ (in 10^{-6})	Err. %	$\overline{f}^{\mathrm{exp}}_{JJ'}$ (in 10^{-6})	$\overline{f}^{\mathrm{calx}}_{JJ'}$ (in 10^{-6})	Err. %	$\overline{f}^{\mathrm{exp}}_{JJ'}$ (in 10^{-6})	$\overline{f}^{\mathrm{calx}}_{JJ'}$ (in 10^{-6})	Err. %
$^4F_{3/2}$	3.83	5.16	30	2.46	3.38	37	1.76	2.14	21	1.34	1.39	4	1.32	2.04	54
$^2H_{9/2}+^4F_{5/2}$	19.83	19.00	4	14.37	13.51	6	10.14	9.85	3	6.04	5.63	7	7.29	6.91	5
$^4S_{3/2}+^4F_{7/2}$	19.98	20.71	4	14.86	15.55	5	11.49	11.73	2	6.04	6.46	7	7.09	7.46	5
$^4F_{9/2}$	1.39	1.60	15	1.14	1.15	1	0.83	0.87	5	0.46	0.47	2	0.65	0.57	12
$^2H_{11/2}$	0.43	0.44	2	0.29	0.32	10	0.22	0.24	9	0.12	0.13	8	0.16	0.16	0
$^2G_{7/2}+^4G_{5/2}$	61.74	61.82	0.1	11.77	11.80	0.2	19.91	19.94	0.1	6.50	6.55	1	6.83	6.89	1
$^4G_{9/2}+^2K_{13/2}+^4G_{7/2}$	16.16	14.84	10	8.30	7.87	5	6.58	6.29	4	4.24	3.50	17	5.27	4.42	16
$^4G_{11/2}+^2G_{9/2}+^2D_{3/2}+^2K_{15/2}$	3.45	3.13	10	2.34	2.14	8	1.59	1.49	6	1.26	0.94	25	1.61	1.18	27
$^2P_{1/2}+^2D_{5/2}$	1.41	1.34	5	0.79	0.83	5	0.53	0.50	6	0.24	0.36	5	0.43	0.54	25
Ω_2 (10^{-20} cm^2)		12.0±0.2			0.4±0.3			4.2±0.1			0.93			0±0.1	
Ω_4 (10^{-20} cm^2)		6.3±0.2			4.8±0.3			2.7±0.1			2.56			3.2±0.1	
Ω_6 (10^{-20} cm^2)		10.1±0.2			9.6±0.3			7.0±0.1			4.98			4.3±0.1	
Ref.		this work			this work			this work			21			this work	

$$\overline{f}^{\mathrm{exp}}_{JJ'}=\frac{f^{\mathrm{exp}}_{JJ'}(\pi)+2\,f^{\mathrm{exp}}_{JJ'}(\sigma)}{3}. \tag{13}$$

The calculated oscillator strengths are determined from the Judd-Ofelt approach.[9,10] The electric dipole oscillator strength of a $J\rightarrow J'$ transition of average frequency v is given by the general expression[9,10]

$$f^{\mathrm{calc}}_{JJ'}=\frac{8\pi^2 m v}{3h(2J+1)e^2}\,\frac{\chi_{ed}}{n}\,S_{ed}(J,J'), \tag{14}$$

where $\chi_{ed}=(n^2+2)^2/9$ is the Lorentz local field correction, n being the refractive index of the host, and S_{ed} is the electric dipole line strength given by

$$S_{ed}(J,J')=e^2\sum_{t=2,4,6}\Omega_t|\langle J\|U^{(t)}\|J'\rangle|^2, \tag{15}$$

where $\Omega_2,\Omega_4,\Omega_6$ are the three Judd-Ofelt parameters[9,10] obtained from fitting calculated oscillator strengths to the experimental values. The reduced matrix elements of the unit tensor operators $U^{(t)}$ are considered to be insensitive to the ion environment.[20]

To a first approximation, the refractive index is considered to be constant across the visible spectrum with the following values: $n_\sigma=1.95$, 1.72, 1.78, 1.45 and $n_\pi=2.16$, 1.82, 1.88, 1.47 for YVO_4, YPO_4, $YAsO_4$, and $LiYF_4$, respectively; and $n_\sigma=n_\pi=1.81$ for $Y_3Al_5O_{12}$. The experimental and calculated oscillator strengths and Judd-Ofelt parameters are reported in Table III. A strong discrepancy is observed between the calculated and the experimental oscillator strengths for the $^4I_{9/2}\rightarrow{}^4F_{3/2}$ transition (30%, 37%, 21%, 54% for YVO_4, YPO_4, $YAsO_4$, and $Y_3Al_5O_{12}$, respectively). The experimental oscillator strengths in the spectral range around 880 nm, at the limit between the visible and near infrared detectors, are underestimated with our experimental set up.

A good agreement is found between the experimental and predicted values for the other transitions (4% to 15% discrepancies for the three hosts). The discrepancy is more important for $Y_3Al_5O_{12}$ because the crystal-field strength experienced by the neodymium ions is two times higher in the garnet than in the zircon-type crystals.[5] For the latter host, several neodymium absorption transitions present a large overlap (for instance, the $^4I_{9/2}\rightarrow{}^2H_{9/2}+{}^4F_{5/2}$; $^4S_{3/2}+{}^4F_{7/2}$ transitions are present in a very narrow energy range). This is also the case for the $^4I_{9/2}\rightarrow{}^4G_{9/2}+{}^2K_{13/2}+{}^4G_{7/2}$; $^4G_{11/2}+{}^2G_{9/2}+{}^2D_{3/2}+{}^2K_{15/2}$ transitions. It is therefore difficult to calculate the individual oscillator strengths in these cases.

Comparing the Judd-Ofelt parameters values obtained for the five hosts (Table III), the Ω_6 parameter increases in the series $Y_3Al_5O_{12}<LiYF_4<YAsO_4<YPO_4<YVO_4$. The Ω_4 parameter follows the same variation for the $Y_3Al_5O_{12}$, YPO_4, YVO_4 hosts. These two phenomenological parameters are very important for the intensity of the $^4F_{3/2}\rightarrow{}^4I_{11/2}$ transition around 1.06 μm since the reduced matrix element of the unit tensor operator $U^{(2)}$ for this transition vanishes.[20] Consequently, the fluorescence intensity around 1.06 μm increases with these parameters. Therefore, the neodymium emission cross section around 1.06 μm in the

TABLE IV. Experimental value of the oscillator strengths $f_{JJ'}^{\text{corr}}$ for Nd^{3+} ions in YMO_4 (M=V, P, As), $Y_3Al_5O_{12}$, and $LiYF_4$, corrected from the host refractive index and the ''hypersensitivity.''

Level	YVO_4	YPO_4	$YAsO_4$	$LiYF_4$	$Y_3Al_5O_{12}$
	$f_{JJ'}^{\text{corr}}$ (in 10^{-6})	$f_{JJ'}^{\text{corr}}$ (in 10^{-6})	$f_{JJ'}^{\text{corr}}$ (in 10^{-6})	$f_{JJ'}^{\text{corr}}$ (in 10^{-6})	$f_{JJ'}^{\text{corr}}$ (in 10^{-6})
$^4F_{3/2}$	1.84	1.49	1.02	1.03	0.77
$^2H_{9/2}+{}^4F_{5/2}$	9.36	8.74	5.82	4.65	4.24
$^4S_{3/2}+{}^4F_{7/2}$	9.72	9.0	6.65	4.66	4.13
$^4F_{9/2}$	0.64	0.68	0.47	0.35	0.38
$^2H_{11/2}$	0.19	0.18	0.12	0.09	0.09
$^2G_{7/2}+{}^4G_{5/2}$	8.67	6.47	3.76	3.33	3.97
$^4G_{9/2}+{}^2K_{13/2}+{}^4G_{7/2}$	6.21	5.01	3.22	3.14	3.07
$^4G_{11/2}+{}^2G_{9/2}+{}^2D_{3/2}+{}^2K_{15/2}$	1.63	1.42	0.90	0.97	0.94
$^2P_{1/2}+{}^2D_{5/2}$	0.67	0.47	0.30	0.18	0.25

three zircon-type crystals is higher than in the two $Nd:Y_3Al_5O_{12}$ and $Nd:LiYF_4$ matrices.

To compare the neodymium oscillator strengths in the different matrices studied in this paper, two host dependent corrections must be taken into account in the experimental oscillator strengths: (i) effects due to the variation of the refractive index between the different compounds and (ii) effects from the ''hypersensitivity'' of some neodymium transitions. In Eq. (14), the refractive index appears in the oscillator strength expression with the Lorentz local field correction. Therefore, the effect of the refractive index on the oscillator strength[22] could be suppressed by using a $n/(\chi_{ed})$ correction factor. The transitions occurring with selection rules $|\Delta J|\leqslant 2$, $|\Delta L|\leqslant 2$ and $\Delta S=0$ are called ''hypersensitive'' transitions.[23] It has been shown that these transitions are strongly related and dominated by the Ω_2 Judd-Ofelt parameter.[23] This parameter is dependent on the local environment of the rare earth and in particular on the ligand polarizability.[24,25] According to previous work,[24–28] the vibrational modes of the host (in particular the odd vibrational modes) contribute to an increase of the Ω_2 parameter. In other work,[22,23,25,29] the ''hypersensitivity'' of the $4f$ transitions is attributed to an inhomogeneity of host dielectric constant, which leads to so-called ''pseudoquadrupole'' transitions presenting the same selection rules as the $\langle J\|U^{(2)}\|J'\rangle$ reduced matrix elements. From Table III, the Ω_2 parameter varies significantly from one host to another ($\Omega_2=0$ and 12×10^{-20} cm^2 for YVO_4 and $Y_3Al_5O_{12}$, respectively), revealing large local modification on the rare-earth environment. The so-called ''hypersensitive'' contribution from the Nd^{3+} transition is proportional to the $\Omega_2|\langle J\|U^{(2)}\|J'\rangle|^2$ product. By taking into account these two host effects, we defined a corrected oscillator strength, $f_{JJ'}^{\text{corr}}$, given by

$$f_{JJ'}^{\text{corr}}=\frac{n}{\chi_{ed}}\left[f_{JJ'}^{\text{exp}}-\frac{8\pi^2 m\nu}{3h(2J+1)}\Omega_2|\langle J\|U^{(2)}\||J'\rangle|^2\right]. \quad (16)$$

The values of $f_{JJ'}^{\text{corr}}$ are reported in Table IV for the different transitions in all the matrices. The oscillator strengths increase in the sequence $Y_3Al_5O_{12}<LiYF_4<YAsO_4<YPO_4<YVO_4$, and they are two times higher in $Nd:YVO_4$ than in $Nd:Y_3Al_5O_{12}$. This increase is global and occurs for all the neodymium transitions.

All the previous mechanisms (effect of odd vibrational modes, pseudoquadrupole transition,...) cannot explain the variation among the hosts, as these mechanisms mostly affect the hypersensitivity of the transition. In the following part of this paper, we attempt to correlate the variation of the oscillator strengths to the rare-earth-matrix interactions and, in particular, to rare-earth-VB covalent interactions.

V. CORRELATION BETWEEN RARE-EARTH VALENCE-BAND INTERACTIONS AND THE OSCILLATOR STRENGTHS OF NEODYMIUM

In the Judd-Ofelt theory,[9,10] the $4f$ transitions are due to a direct interaction between the $4f^n$ and excited $4f^{n-1}\alpha 1$ ($\alpha 1=5d,6s$) configurations of even parity, in particular, the $4f^{n-1}5d$ configuration, which is the first excited configuration. This configuration interaction is due to the contribution of an odd crystal-field term in a perturbation treatment, which leads to nonzero matrix elements of the electric dipole-moment operator between the mixed-parity wave functions.

The approach derived in this paper is based on an indirect interaction between the $4f^n$ and $4f^{n-1}5d$ configurations, where the $5d$ levels are mixed with the $4f$ levels via the VB states by the two-step mechanism described in Fig. 1: (i) From a band-structure calculation performed on the undoped matrix[30] the d-metal levels (in YVO_4, the yttrium $4d$ and vanadium $3d$ levels) are found to interact with the valence-band levels, which leads to a $3d$ and $4d$ admixture into the VB states. As the neodymium $5d$ levels in the doped matrix are close to the conduction-band edge, which is essentially of d metal character, there is also a $5d$ neodymium admixture into the VB levels. (ii) This Nd $5d$ admixture into the VB is transmitted to the Nd $4f$ levels via the $4f$-VB interaction identified by XPS in Sec. IV.

This two-step $4f$-$5d$ mixing mechanism may result in an

enhanced $4f$-$4f$ transition probability. Let us consider two J,J' levels, where $J=\frac{9}{2}$ is the fundamental $^4I_{9/2}$ multiplet of Nd^{3+} ions and J' is an excited multiplet of the $4f^3$ configuration. $|\varphi_{VB}\rangle$ is a wave function associated with a valence-band level interacting with the $4f$ shell. The energy splitting, derived from $3d$ XPS, between the fundamental J state of the $4f$ levels and the valence-band state $|\varphi_{VB}\rangle$ is $E_{4f}-E_{VB}$. As previously shown, the orbital interaction V, representing the mixture of this valence-band state with the fundamental J state, is very weak. This admixture can, thus, be estimated by a first-order perturbation expressions

$$|J\rangle=|J^0\rangle+\frac{V}{E_J^0-E_{VB}}|\varphi_{VB}\rangle, \tag{17}$$

$$|J'\rangle=|J'^0\rangle+\frac{V}{E_J'^0-E_{VB}}|\varphi_{VB}\rangle, \tag{18}$$

where $|J_0\rangle$ and $|J_0'\rangle$ are the wave functions of the free $4f$ states and E_J^0 and $E_{J'}^0$ the associated zero-order energies. The matrix element of the electric dipole moment operator P is then written as

$$\langle J|P|J'\rangle=\langle J^0|P|J'^0\rangle+\frac{V}{E_J^0-E_{VB}}\langle J^0|P|\varphi_{VB}\rangle + \frac{V}{E_J'^0-E_{VB}}\langle J'^0|P|\varphi_{VB}\rangle. \tag{19}$$

Equation (19) can be simplified as follows: first the $\langle J^0|P|J'^0\rangle$ matrix element vanishes as the $|J_0\rangle$ and $|J_0'\rangle$ states are purely $4f$ states; second, the energy splitting $E_J^0-E_{VB}$ is equal to $E_{4f}-E_{VB}$ measured from $3d$ XPS. For all the matrices, the energy splitting of the $4f^3$ configuration, due to Coulomb, spin-orbit, and crystal-field interactions, is not negligible compared with $E_{4f}-E_{VB}$, which implies $E_{J'}^0-E_{VB}=(E_{4f}-E_{VB})+E_{JJ'}$, where $E_{JJ'}$ is the energy of the $^4I_{9/2}\rightarrow{}^{2S'+1}L_{J'}$ transition measured from absorption spectra; third, the Nd $5d$ levels are mixed with the VB states by a metal-anion covalency, $|\varphi_{VB}\rangle$ is then a linear combination of VB $2p$ states and Nd $5d$ states, which could be written as $|\varphi_{VB}\rangle=c|2p\rangle+d|5d_{Nd}\rangle$ with $d\neq 0$. Thus, the matrix elements of P in Eq. (19) are reduced to

$$\langle J^0|P|\varphi_{VB}\rangle=d\langle J^0|P|5d_{Nd}\rangle\neq 0. \tag{20}$$

By assuming that $\langle J^0|P|\varphi_{VB}\rangle=\langle J'^0|P|\varphi_{VB}\rangle$, and the value of d does not vary significantly, the oscillator strengths $f_{JJ'}$ obtained from this two-steps admixture mechanism are therefore written as

$$f_{JJ'}\propto\frac{V^2}{(E_{4f}-E_{VB})^2}\left(\frac{2+\dfrac{E_{JJ'}}{E_{4f}-E_{VB}}}{1+\dfrac{E_{JJ'}}{E_{4f}-E_{VB}}}\right)^2, \tag{21}$$

where all of the parameters of Eq. (21) are measured experimentally.

To compare the corrected oscillator strengths $f_{JJ'}^{corr}$, measured experimentally, to the oscillator strengths $f_{JJ'}$, calculated from Eq. (21) for each host and each neodymium transition, values are normalized with respect to those of Nd^{3+} ions in YVO_4

$$f_{JJ'}^{corr}(\text{norm.})=\frac{f_{JJ'}^{corr}}{f_{JJ'}^{corr}(YVO_4)}, \qquad f_{JJ'}(\text{norm.})=\frac{f_{JJ'}}{f_{JJ'}(YVO_4)}, \tag{22}$$

and for the sake of comparison we calculate an average oscillator strength given by

$$\overline{f}^{corr}(\text{norm.})=\frac{1}{i}\sum_i f_{JJ'}^{corr}(\text{norm.}), \qquad \overline{f}(\text{norm.})=\frac{1}{i}\sum_i f_{JJ'}(\text{norm.}), \tag{23}$$

where i is the ith Nd^{3+} $4f$ transition. The values of the oscillator strengths $f_{JJ'}^{corr}$(norm.), $f_{JJ'}$(norm.), $\overline{f}^{corr}$(norm.), and $\overline{f}$(norm.) are reported in Table V. Figure 7 represents the variation of the calculated oscillator strengths $\overline{f}$(norm.) versus the experimental oscillator strengths $\overline{f}^{corr}$(norm.) for the $Y_3Al_5O_{12}$, $LiYF_4$, $YAsO_4$, YPO_4, and YVO_4 matrices (all of the values are normalized to those of the YVO_4 compound). A unit slope represents the ideal situation, where the variation of the oscillator strengths across the series is only due to the Nd-matrix covalency effect. Despite a significant discrepancy between the calculated points and the ideal situation, it is clear that the oscillator strengths increase from the more ionic to the more covalent compounds.

These results indicate that there is a relationship between the variation of the Nd-valence-band interactions and the variation of the rare-earth oscillator strengths. An increase of the $4f$-valence-band and $5d$ valence-band interactions leads to an increase of the Nd^{3+} oscillator strengths.

It is worth noting that we only considered the Nd-VB interactions and completely neglected Nd-conduction-band (CB) interactions, although the latter should exist for several reasons. Rare-earth–CB interactions have been experimentally observed from multiphoton absorption and excited-state absorption in $Y_3Al_5O_{12}$.[31,32] Nd $5d$ levels are close to the conduction-band edge, so that direct Nd $5d$-CB interactions should be effective. Because of the more diffuse character of $5d$ orbitals compared to $4f$ orbitals and the Y $4d$ orbital characteristics of the conduction-band edges in $LiYF_4$, YPO_4, and $YAsO_4$ and V $3d$ orbitals in YVO_4,[30] one should expect direct Nd-CB interactions via Nd $5d$-Y $4d$ or Nd $5d$-V $3d$ interactions. Although a detailed investigation of these effects is beyond the scope of this paper, it is, however, possible to briefly analyze their possible influence on the strength of the Nd^{3+} optical transitions.

Within the framework of the Judd-Offelt theory, the electric-dipole forbidden $4f$-$4f$ transitions are slightly allowed by some even parity admixture to $4f$ states by the effect of the odd terms V_{odd} of the crystal-field Hamiltonian. This odd parity admixture is simply accounted for by a first-order perturbation expression

TABLE V. Normalized values of the experimental [$f_{JJ'}^{corr}$(norm.)], calculated [$f_{JJ'}$(norm.)], oscillator strengths of Nd^{3+} ions in YMO_4 (M=V, P, As), $Y_3Al_5O_{12}$, and $LiYF_4$ corrected from host effects (refractive index and ''hypersensitivity''). f^{corr}(norm.) and $\overline{f}$(norm.) are the corresponding values average over all the $4f$-$4f$ transitions.

	YVO_4		YPO_4		$YAsO_4$		$LiYF_4$		$Y_3Al_5O_{12}$
Level	$f_{JJ'}^{corr}$(norm.)	$f_{JJ'}$(norm.)	$f_{JJ'}^{corr}$(norm.)	$f_{JJ'}$(norm.)	$f_{JJ'}^{corr}$(norm.)	$f_{JJ'}$(norm.)	$f_{JJ'}^{corr}$(norm.)	$f_{JJ'}$(norm.)	$f_{JJ'}$(norm.)
$^4F_{3/2}$	1	1.00±0.09	0.81	0.83±0.08	0.55	0.64±0.07	0.56	0.35±0.02	0.42	0.29±0.02
$^2H_{9/2}+{}^4F_{5/2}$	1	1.00±0.09	0.93	0.84±0.08	0.63	0.64±0.07	0.50	0.35±0.02	0.45	0.29±0.02
$^4S_{3/2}+{}^4F_{7/2}$	1	1.00±0.09	0.93	0.84±0.08	0.68	0.64±0.07	0.48	0.35±0.02	0.42	0.29±0.02
$^4F_{9/2}$	1	1.00±0.09	1.04	0.84±0.08	0.73	0.64±0.07	0.54	0.35±0.02	0.59	0.29±0.02
$^2H_{11/2}$	1	1.00±0.09	0.9	0.83±0.08	0.60	0.64±0.07	0.45	0.35±0.02	0.45	0.29±0.02
$^2G_{7/2}+{}^4G_{5/2}$	1	1.00±0.09	0.74	0.83±0.08	0.43	0.64±0.07	0.38	0.35±0.02	0.46	0.29±0.02
$^4G_{9/2}+{}^2K_{13/2}+{}^4G_{7/2}$	1	1.00±0.09	0.81	0.83±0.08	0.52	0.64±0.07	0.50	0.36±0.02	0.49	0.30±0.02
$^4G_{11/2}+{}^2G_{9/2}+{}^2D_{3/2}+{}^2K_{15/2}$	1	1.00±0.09	0.87	0.83±0.08	0.55	0.65±0.07	0.59	0.36±0.02	0.57	0.30±0.02
$^2P_{3/2}+{}^2D_{5/2}$	1	1.00±0.09	0.70	0.84±0.08	0.45	0.65±0.07	0.27	0.36±0.02	0.37	0.30±0.02
$\overline{f}^{corr}$(norm.)	1		0.86		0.57		0.47		0.46	
$\overline{f}$(norm.)	1.00±0.09		0.83±0.08		0.64±0.07		0.35±0.02		0.29±0.02	

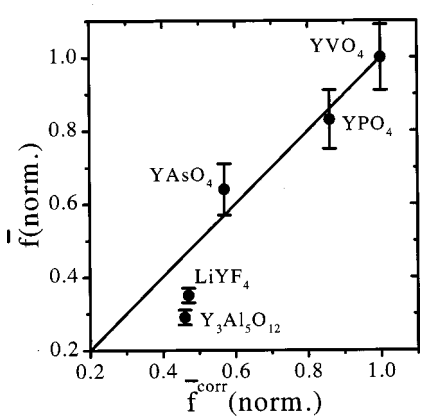

FIG. 7. Variation of the calculated oscillator strength $\overline{f}$(norm.) versus the experimental oscillator strength $\overline{f}^{corr}$(norm.) of Nd^{3+} ions in YMO_4 (M=V, P, As), $Y_3Al_5O_{12}$, and $LiYF_4$, averaged over all the Nd^{3+} transitions. All the values are normalized with respect to YVO_4. The straight line represents a perfect agreement between the two sets of parameters.

$$|4f'\rangle = |4f\rangle + \sum \frac{\langle 5d|V_{odd}|4f\rangle}{E_{4f}^{(0)} - E_{5d}^{(0)}}|5d\rangle, \tag{24}$$

where $E_{4f}^{(0)}$ and $E_{5d}^{(0)}$ are the unperturbed $4f$ and $5d$ energy levels. Let us consider a conduction-band level (with Y $4d$ or V $3d$ character) of energy E_{CB} with $E_{5d}^{(0)} < E_{CB}$ [case (i)]. A covalent interaction between Nd $5d$ and CB levels shifts the former to lower energy because of its bonding character. In turn, the energy splitting $E_{4f}^{(0)} - E_{5d}^{(0)}$ in Eq. (24) is reduced and the effect of the even-parity admixture into $4f$ states is enhanced with a resulting increased of the oscillator strengths. Alternatively, the opposite effect is expected for $E_{5d}^{(0)} > E_{CB}$ [case (ii)], where the antibonding character of the Nd $5d$ level leads to an increase in the energy splitting $E_{4f}^{(0)} - E_{5d}^{(0)}$. We thus expect an increase of $4f$-$4f$ transition strengths in compounds with large energy gaps $E_g > E_{4f}^{(0)} - E_{5d}^{(0)}$. Compounds such as $YLiF_4$ (E_g=10.1 eV), $Y_3Al_5O_{12}$ (E_g=6.9 eV), and YPO_4 (E_g=8.3 eV) correspond to case (i), while $YAsO_4$ (E_g=6.8 eV) and YVO_4 (E_g=3.6 eV) correspond to case (ii).[30] It is interesting to note that the experimental points in Fig. 7 lie below the ideal line (increased of the transitions strengths) for $YLiF_4$, $Y_3Al_5O_{12}$, and YPO_4 and above this line for $YAsO_4$. Considering the experimental uncertainties, it is, however, not possible to come to a definitive conclusion as to the effect of Nd-CB interactions on the Nd oscillator strengths.

VI. CONCLUSION

We have presented an analysis of the covalent interactions between rare-earth and VB levels and their effects on the neodymium $4f$ transition intensity. The neodymium oscillator strengths in YMO_4 (M=V, P, As), $Y_3Al_5O_{12}$, $LiYF_4$ have been measured and corrected for host effects (refractive index and ''hypersensitivity''). The oscillator strengths are found to increase in the sequence $Y_3Al_5O_{12} < LiYF_4 < YAsO_4 < YPO_4 < YVO_4$.

Interactions between Nd $4f$ levels and VB levels have been estimated by photoelectron spectroscopy. The strengths

of these covalent interaction were estimated from neodymium $3d$ XPS spectra. The $4f$-VB covalency appears to increase from the more ionic compound ($LiYF_4$) to the more covalent one (YVO_4).

A model is proposed on the basis of a correlation between the oscillator strength and the $4f/5d$-VB interactions. In this approach, an admixture of Nd $5d$ and VB levels results in a $4f$-$5d$ mixing via the $4f$-VB interaction measured by XPS. Therefore, an odd $5d$ character is admixed into the even $4f$ levels via the Nd-matrix covalency, enhancing the parity-forbidden $4f$ transitions.

This approach is, however, based on two several assumptions: (i) The $(U_{fd}-3U_{ff})$ term, containing the Coulomb interaction between $4f$ electrons U_{ff} and the core-hole potential acting on the $4f$ electrons U_{fd}, does not vary significantly from Nd metal to Nd_2O_3. It would be necessary to measure precisely these values for Nd_2O_3. (ii) The admixture of Nd-$5d$ levels into the VB levels is almost constant from one host to another. It would be necessary to verify this assumption by band structure calculations on doped matrices. However, it seems that this very simple approach reproduces rather well the experimental variations of neodymium oscillator strengths across the series of matrices.

ACKNOWLEDGMENTS

The authors are grateful to DGA for financial support. We wish to thank Dr. B Ferrand (LETI-CEA) and M. Queffellec (Institut de Physique Nucléaire, Orsay) for providing us, respectively, with the Nd^{3+}:YVO_4 and the Nd^{3+}:$LiYF_4$ crystals used in this work. One of us (O.G.N.) is indebted to C. Combes for fruitful discussions. We also thank S. Jobic and G. Gauthier from the IMN of Nantes for the band-structure calculations on the undoped matrices.

[1] D. G. Matthews, J. R. Boon, R. S. Conroy, and B. D. Sinclair, J. Mod. Opt. **43**, 1079 (1996).
[2] B. H. T. Chai, G. Loutts, J. Lefaucheur, X. X. Zhang, P. Hong, M. Bass, I. A. Shesherbakov, and A. I. Zagumennyi, OSA Proc. Adv. Solid-State Lasers **20**, 41 (1994); A. A. Kaminskii, G. A. Bogomolova, and L. Li, Inorg. Mater. **5**, 573 (1969).
[3] G. Feugnet, C. Bussac, C. Larat, M. Schwarz, and J. P. Pocholle, Opt. Lett. **20**, 157 (1995).
[4] O. Guillot-Noël, B. Viana, G. Aka, D. Gourier, A. Kahn-Harari, and D. Vivien, J. Lumin. **72-74**, 195 (1997).
[5] O. Guillot-Noel, A. Kahn-Harari, B. Viana, D. Vivien, E. Antic-Fidancev, and P. Porcher, J. Phys.: Condens. Matter **10**, 6491 (1998).
[6] O. L. Malta, Chem. Phys. Lett. **88**, 353 (1982).
[7] P. Porcher, M. Couto Dos Santos, and O. L. Malta, Phys. Chem. Chem. Phys. **1**, 397 (1999).
[8] C. K. Jorgensen, *Absorption Spectra and Chemical Bonding in Complexes* (Pergamon, New York, 1962).
[9] G. S. Ofelt, J. Chem. Phys. **37**, 511 (1962).
[10] B. R. Judd, Phys. Rev. **127**, 750 (1962).
[11] A. Katoni and H. Ogasawara, J. Electron Spectrosc. Relat. Phenom. **60**, 257 (1992).
[12] A. Kotani, T. Jo, and J. C. Parlebas, Adv. Phys. **37**, 37 (1988).
[13] J. C. Parlebas, E. Beaurepaire, T. Ikeda, and A. Kotani, J. Phys. (France) **51**, 639 (1990).
[14] J. C. Parlebas, T. Nakano, and A. Kotani, J. Phys. (Paris) **48**, 1141 (1987).
[15] H. Bertou, C. K. Jorgensen, and C. Bonnelle, Chem. Phys. Lett. **38**, 19 (1976).
[16] P. W. Anderson, Phys. Rev. **124**, 41 (1961).
[17] P. A. Cox, J. K. Lang, and Y. Baer, J. Phys. (Paris) **37**, 671 (1976).
[18] B. T. Hole, G. van Der Laan, J. C. Fuggle, G. A. Sawatzky, R. G. Karnatak, and J. M. Esteva, Phys. Rev. B **32**, 5107 (1985).
[19] G. Kaindl, G. Kalkowski, W. D. Brewer, B. Perscheid, and F. Holtzberg, J. Appl. Phys. **55**, 1910 (1984).
[20] A. A. Kaminskii, *Crystalline Lasers: Physical Processes and Operating Schemes* (CRC, Boca Raton, 1996).
[21] Y. Guyot, Ph.D. thesis, Université Claude Bernard–Lyon I, 1993.
[22] F. Auzel, Ann. Telecommun. **24**, 199 (1969); Ph.D. thesis, Faculté des Sciences–Paris, 1968
[23] C. K. Jorgensen and B. R. Judd, Mol. Phys. **8**, 281 (1964).
[24] C. K. Jorgensen and R. Reisfeld, J. Less-Common Met. **93**, 107 (1983).
[25] R. Reisfeld and C. K. Jorgensen, *Laser and Excited States of Rare Earth* (Springer-Verlag, Berlin, 1977).
[26] J. Dexpert-Ghys and F. Auzel, J. Chem. Phys. **80**, 4003 (1984).
[27] G. Blasse, Int. Rev. Phys. Chem. **11**, 71 (1992).
[28] O. Malta, J. Phys. Chem. Solids **56**, 1053 (1995).
[29] R. D. Peacok, Struct. Bonding (Berlin) **83**, (1973).
[30] O. Guillot-Noel, Ph.D. thesis, Université Pierre et Marie Curie, Paris, 1998.
[31] M. Kramer and R. Boyd, Phys. Rev. B **23**, 986 (1981); S. K. Gayen and B. Q. Xie, J. Opt. Soc. Am. B **10**, 993 (1993).
[32] D. S. Hamilton, S. K. Gayen, G. J. Pogatshnik, R. D. Ghen, and W. J. Miniscalco, Phys. Rev. B **39**, 8807 (1989); Y. M. Cheung and S. K. Gayen, *ibid.* **49**, 14 827 (1994)